Clays and Clay Minerals, Vol. 66, No. 4, 353–369, 2018.

QUANTITATIVE MINERALOGY OF CLAY-RICH SILICICLASTIC LANDSLIDE TERRAIN OF THE SORRENTO PENINSULA, ITALY, USING A COMBINED XRPD AND XRF APPROACH

M. Cesarano[1,*], D. L. Bish[2], P. Cappelletti[1], F. Cavalcante[3], C. Belviso[3], and S. Fiore[3]

[1] DiSTAR, Università degli Studi di Napoli Federico II, 80134 Napoli, Italy,
[2] Dept. of Geological Sciences, Indiana University, 47405 Bloomington, Indiana, USA
[3] Institute of Methodologies for Environmental Analysis-CNR, 85050 Tito Scalo, Potenza, Italy

Abstract—Quantitative mineralogical analysis of clay-bearing rocks is often a non-trivial problem because clay minerals are characterized by complex structures and are often affected by structural disorder, layer-stacking disorder, and interstratification. In the present study, internal-standard Rietveld X-ray powder diffraction (XRPD) analyses were combined with X-ray fluorescence (XRF) chemical analyses for the mineralogical characterization and quantitative analysis of heterogeneous clay-rich sedimentary rocks that are involved in a slow-moving landslide in the Termini-Nerano area, Sorrento Peninsula (Italy), in order to investigate the relationship between the mineralogy of these rocks and landslides. Slow-moving landslides are usually considered to be associated with the more weathered and surficial parts of structurally complex slopes, and mineralogical analysis can help to clarify the degree of weathering of siliciclastic rocks. XRPD quantitative analyses were conducted by combining the Rietveld and internal standard methods in order to calculate the amounts of poorly ordered phyllosilicate clays (considered amorphous phases in Rietveld refinements) by difference from 100%. The *vbAffina* program was used to refine the amounts of mineral phases determined with XRPD using the element compositions determined by XRF analysis. XRPD analyses indicated that the samples mainly contain several different clay minerals, quartz, mica, and feldspars. Analysis of the clay fraction identified kaolinite, chlorite, and interstratified illite-smectite (I-S) and chlorite-smectite (C-S). The mineralogy of the materials involved in the landslide in comparison with the mineralogy of the "undisturbed" rocks showed that the landslide is located in the weathered realm that overlies an arkosic bedrock. The interstratified I-S and C-S occurred at landslide activity locations and confirmed that areas more susceptible to sliding contained the most weathered parts of the rocks and perhaps represent areas of past and currently active fluid flow.

Key Words—Combined XRF-XRPD Analysis, Internal Standard Rietveld Method, Interstratified I-S and C-S, Landslide, XRPD Quantitative Analysis.

INTRODUCTION

The mineralogical composition of sedimentary rocks depends on the nature of the sediment sources and on processes such as weathering, transport, sedimentation, and diagenesis that have modified the original mineralogy (Środoń, 2002). X-ray powder diffraction (XRPD) is the most popular method used to determine the mineralogy of rocks because it can provide information on the minerals that occur in the rock and can quantify mineral abundances for simple or very complex materials, which includes different phyllosilicates (Brindley, 1980; Snyder and Bish, 1989; Środoń *et al.*, 2001; De Ruan and Ward, 2002; Omosoto *et al.*, 2006; Shen *et al.*, 2012; Dumon *et al.*, 2014). To evaluate the relative amounts of mineral phases, methods based on peak intensity ratios that use an internal standard, a reference intensity ratio (RIR), or the Rietveld method are frequently used. Quantitative phase analysis (QPA) based on the Rietveld method, which fits a simulated pattern based on structural models to measured XRPD data, is an effective method for well-ordered phases (Bish and Howard, 1988; Snyder and Bish, 1989; Chipera and Bish, 2002). Quantifying disordered clay minerals, such as smectite and interstratified phyllosilicates, however, remains more challenging (*e.g.*, Ufer *et al.*, 2008, 2012). Clays occur as discrete minerals (*e.g.*, kaolinite, chlorite) and as interstratifications of different layers along the c* direction (Środoń, 2002). Expandable layers and stacking defects have important effects on XRPD patterns and typically make the Rietveld approach not applicable for rigorous quantitative analysis or structure refinement. To circumvent this difficulty, XRPD quantitative analyses can be combined with chemical data, *e.g.*, whole-rock chemical data directly related to the amounts and chemical compositions of the rock constituents (Ufer *et al.*, 2008). As reported by Snyder and Bish (1989), the use of chemical analyses to calculate the chemical composition of a rock combined with XRPD quantification was first used in the 1950s and became popular in the 1980s. Pearson (1978) and Slaughter (1989) used linear programming and constrained the solution using chemical and

* E-mail address of corresponding author:
mara.cesarano@unina.it
DOI: 10.1346/CCMN.2018.064108

mineralogical XRPD data. Calvert *et al.* (1989) used chemistry as an additional constraint in the least-squares whole-pattern fitting program of Smith *et al.* (1987) and improved the results for artificial mixtures. Most recently, Ufer *et al.* (2008) used XRF data as an independent assessment of the quantitative results that were obtained using Rietveld refinement (for bentonite samples). These studies confirmed that the combination of XRF and XRPD data allows a less biased quantification of poorly ordered mineral phases.

Slow-moving landslides are generally considered to be related to the most weathered and surficial parts of structurally complex formation slopes (Taylor and Cripps, 1987; Calcaterra *et al.*, 2006), which in the engineering geology literature are known as broken formations, scaly clays, chaotic complexes, and variegated clays (Bianconi, 1840; Di Bucci, 1996). Taylor and Cripps (1987) showed that weathering acts on these soils through the formation of "weathering zones" that are characterized by an increase in material degradation from the bottom to the top. The most weathered rocks were assumed to contain the largest amounts of expandable clays (*e.g.*, smectite). One of the phenomena associated with these clays is the ability to adsorb water with concomitant swelling. For this reason, the transition from the dry season (summer) to the cold and rainy season (winter) and back can be marked by shrinkage and swelling phenomena. Based on these assumptions, several authors attempted to determine whether a correlation existed between landslide occurrence and the mineralogical features of the material. Cruden and Varnes (1996) suggested that an increase in water pore pressure may be responsible for decreased shear strength and, thus, represents a crucial factor to determine the onset of slope instability as was verified for the Bisaccia and Agnone landslides (Maggi and Pellegrino, 2002; Maggi, 2003; Calcaterra *et al.*, 2007).

The aims of the present study were to characterize the mineralogy and to quantitatively analyze the heterogeneous clay-rich sedimentary rocks that are involved in a slow-moving landslide in the southern Apennines, near Massalubrense on the Sorrento Peninsula in Southern Italy, in order to evaluate the relationship between rock mineralogy and landslides. For the present study, an internal-standard Rietveld XRPD method combined with chemical XRF analyses was used with a set of samples selected from boreholes drilled in the landslide area. The study area was affected in 1963 by sudden activation of the Termini Nerano landslide, which is a slow moving landslide about 2 km in length. Three villages were involved and damaged by the Termini Nerano landslide, which were the Termini, Nerano, and Marina del Cantone villages that respectively correspond to the landslide crown, slide zone, and accumulation zones (Cotecchia and Melidoro, 1966). The landslide area remains active and the slope is currently affected by a slow retrogressive movement, which corresponds to the crown zone, and paroxysmal events are likely to occur again in the area (Picarelli and Russo, 2004; Cascini *et al.*, 2005; Mansour *et al*., 2011).

GEOLOGICAL SETTING AND LITHOLOGIC CHARACTERISTICS OF THE STUDY AREA

The 1963 Termini Nerano landslide (Figure 1, blue area labeled A) is the result of complex movements (Cotecchia and Melidoro, 1966; Cruden and Varnes, 1996) that began as a slow roto-translational landslide that corresponds to the present-day crown zone and evolved into more rapid flow after triggering events, such as long duration rainfall, which overlapped the 1940 landslide deposits. The 1963 landslide is distinct from the larger slides (the 1940 slide in yellow labeled B and 2011 slide in green labeled D), which are defined as roto-translational slides. The total length of the 1963 Termini Nerano landslide is ~1900 m from the crown zone to the shore at the Marina del Cantone village. As reported by Cotecchia and Melidoro (1966), the 1963 phenomenon involved about 1×10^6 m^3 of materials that were characterized by the alternation of shales and sandstones of the *Arenarie di Termini* Formation. Seismic analyses carried out in the area after the event showed that the deepest slip surface occurred at a depth of about 25 m (Cotecchia and Melidoro, 1966).

In detail, the geology of the Termini and Nerano areas is dominated by the presence of terrains that belong to the Mesozoic-Cenozoic *Monti Lattari Picentini* tectonic unit. Three main sedimentary lithologies occur in the landslide area that belong to the *Calcari a Radiolitidi*, *Calcareniti di Recommone*, and *Arenarie di Termini* Formations (Figure 2). The *Calcari a Radiolitidi* Formation is a succession of dolostones, limestones, and rare calcareous conglomerate interbeds. The *Calcareniti di Recommone* Formation is mainly constituted by bioclastic and glauconitic calcarenites, which through increases in the siliciclastic fraction and decreases in the calcareous component, gradually merge with the overlying *Arenarie di Termini* Formation sandstones (Termini Sandstones) (Iannace *et al.*, 2015). The materials that are mainly involved in the landslide belong to the *Arenarie di Termini* Formation, which is a siliciclastic succession of Miocene age that is stratigraphically continuous over the carbonate lithologies of the *Calcareniti di Recommone* Formation (Iannace *et al.*, 2015). The *Arenarie di Termini* Formation is constituted by red, green, and grey-greenish arkosic sandstones and shales intercalated with calcarenite and marls. Iannace *et al.* (2015) reported that the sandstones that belong to the *Arenarie di Termini* Formation are generally characterized by a low diagenetic grade with abundant detrital quartz and feldspars and minor lithic components. The *Arenarie di Termini* Formation rocks are consequently classified as quartz-feldspar sandstones. The lithic fragments show high diagenetic grades that were

https://doi.org/10.1346/CCMN.2018.064108 Published online by Cambridge University Press

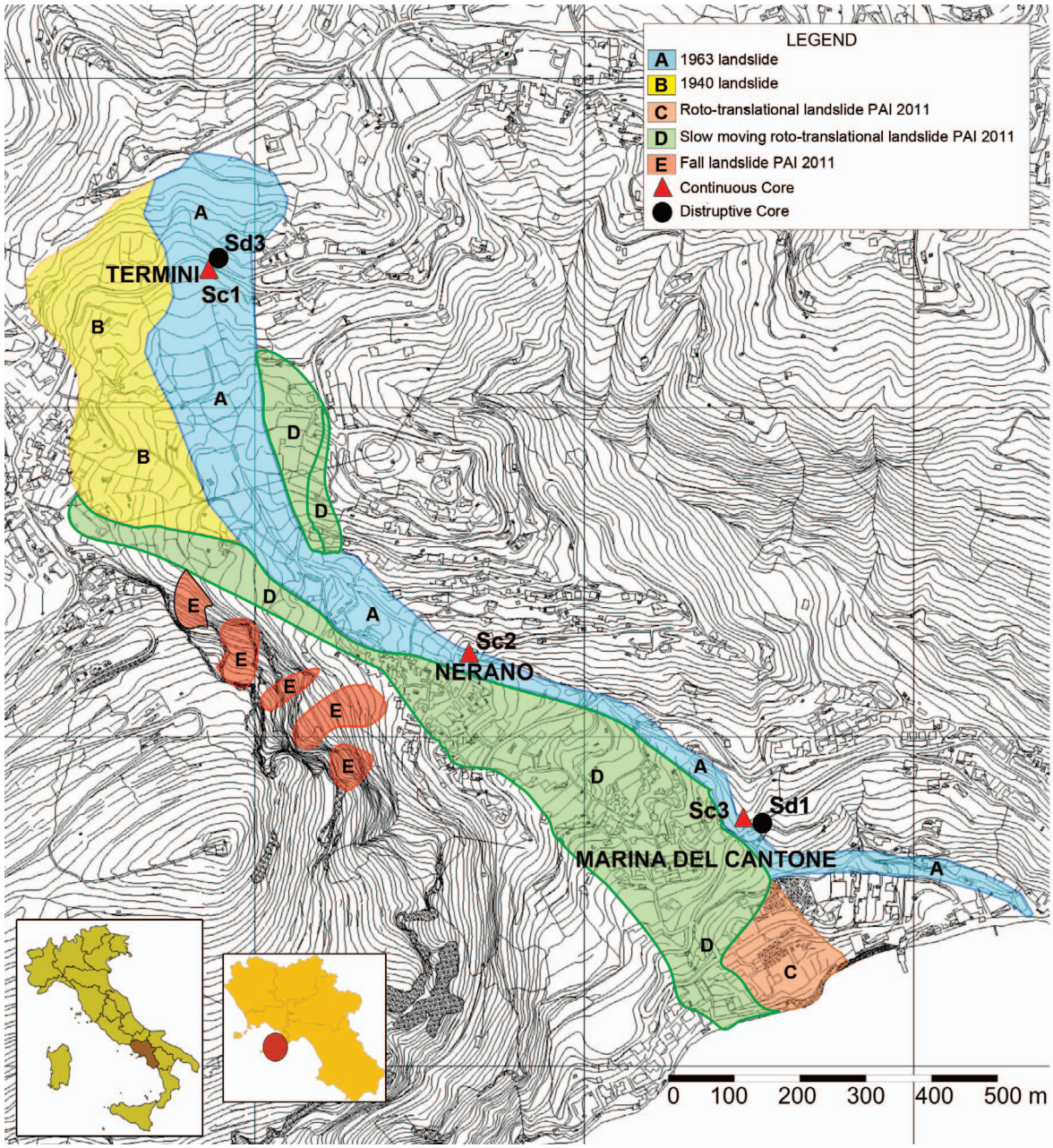

Figure 1. Geomorphological map of the Termini-Nerano area (P.A.I., 2011, modified), with locations of the studied drill cores. The 1963 landslide location is shown in blue (gray in grayscale) marked with the letter A.

inherited from the original parent rocks and eroded at the time as sandstone deposition. In detail, Iannace *et al.* (2015) reported the occurrence of lithic fragments of clear igneous origin, as well as gneiss, slate, phyllite, and rare serpentinite, siltstone, and shale fragments that were derived from the erosion of an orogenic area. At the time of sandstone deposition, the orogenic area was characterized by rapid uplift with a metamorphic basement that was intruded by plutons.

MATERIALS AND METHODS

Twenty-six samples (Table 1) were selected from three cores drilled into the Termini sandstones that corresponded to the crown zone, the sliding zone, and the accumulation zone of the 1963 Termini Nerano landslide (Figure 1). Both qualitative and quantitative mineralogical analyses were performed on the selected samples. Qualitative analyses were carried out on bulk samples and on clay fractions separated from the bulk samples. Specific analyses of interstratified phyllo-

https://doi.org/10.1346/CCMN.2018.064108 Published online by Cambridge University Press

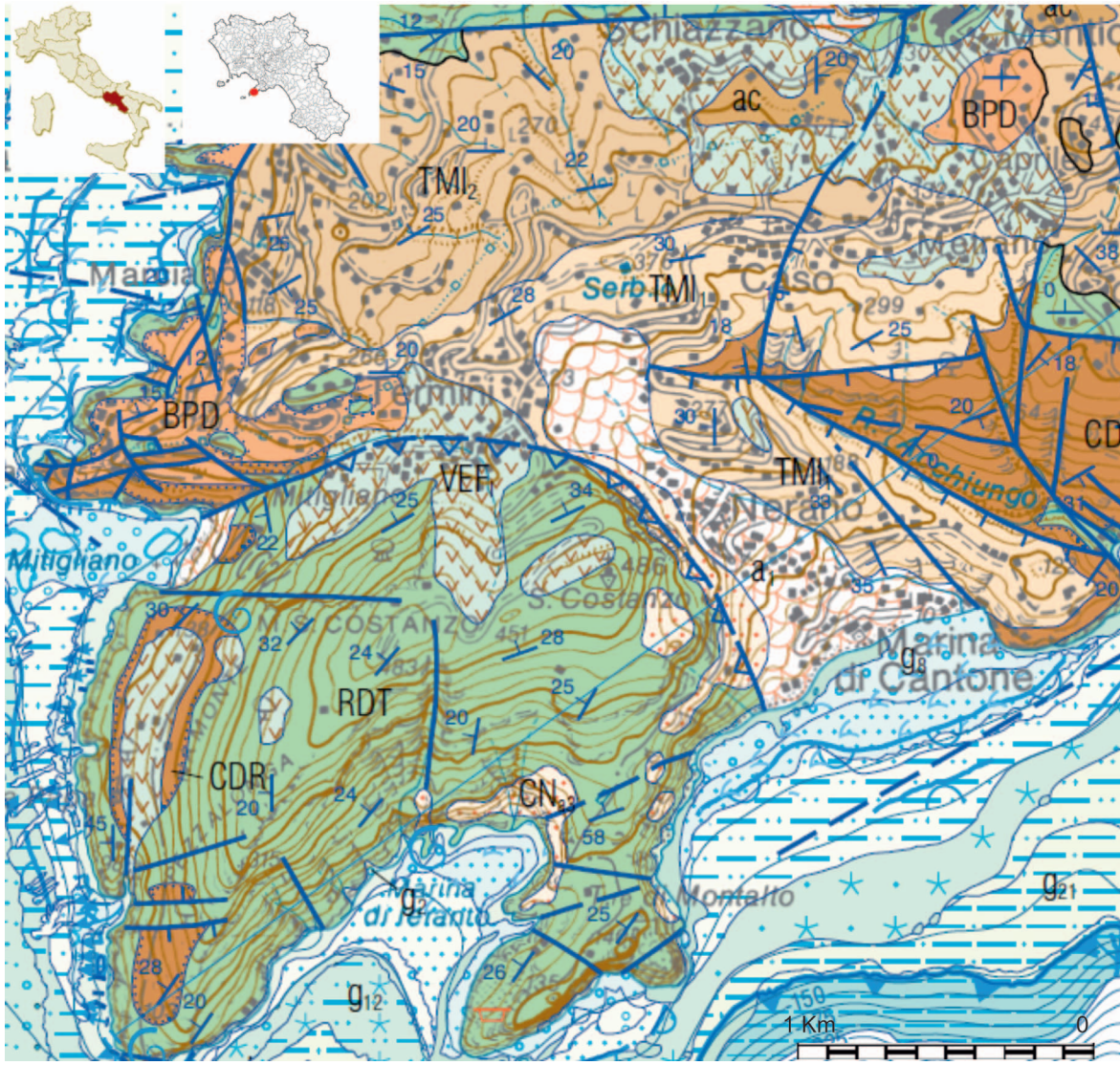

Figure 2. Geological map of the Termini-Nerano area (Iannace et al., 2015, modified). $TM1_1$ = Termini sandstone, CDR = Calcareniti di Recommone, RDT = Calcari a Radiolitidi, a_1 = landslide deposits, BOD = Breccia di Punta del Capo, VEF_1 = Vesuvian Flegrean Synthem.

silicates were performed to evaluate the component layers as well as the Reichweite (R value) layer stacking order (Moore and Reynolds, 1997). Quantitative mineral analyses were carried out on bulk samples by combining XRPD quantitative analysis and whole rock chemical data determined using XRF analysis (Table 2).

Both major and trace element XRF analyses were obtained using PANalytical Axios instruments (PANalytical, Amelo, The Netherlands) at the Dipartimento di Scienze della Terra, dell'Ambiente e delle Risorse (DiSTAR), at the University of Naples Federico II, Napoli, and at the Department of Earth and Geo-environmental Sciences at Aldo Moro University, Bari, controlled using *Super Q 4.0J.L* software. Four-gram samples were crushed in an agate mortar, mixed with polyvinyl alcohol (at 10 wt.%.), and oven dried at 50ºC for 48 h. This material was placed in a metal sample holder, which was about ½ full of granular boric acid and was pressed into a pellet at ~18 atm for ~20 sec. The loss on ignition (LOI) represented the mass loss due to H_2O and CO_2 lost during firing the sample at 1100ºC for 2 h. The XRPD analyses were carried out using several different instruments: (1) a Rigaku DMax 2200 (Rigaku Corporation, Tokyo, Japan) (CNR-IMAA, Tito Scalo, Potenza) with measurement conditions of CuKα radiation, 40 kV, 30 mA, scintillation detector, measured from 2–70º2θ, 0.02º2θ steps, and a 2 s/step count time; (2) a Bruker D8 Advance (Bruker, Billerica, Massachusetts, USA) at Dept. of Geological Sciences, Indiana University with measurement conditions of

https://doi.org/10.1346/CCMN.2018.064108 Published online by Cambridge University Press

Table 1. List of samples analysed in this study.

ID sample	Depth (m)	Lithology
PN1	3.3	Sand
PN2	4.7	Silty clay
PN3	7	Marly clay
PN4	8.9	Calcarenitic sandstone
PN5	14	Marly shale
PN6	16.5	Marly shale
PN7	18.5	Marly shale
PN8	23	Marly shale
PN9	24.9	Marly shale
PR1	3	Silty shale
PR2	4.5	Silty shale
PR3	6	Clayey silt
PR5	9.7	Sandstone
PR6	11	Sandstone
PR7	14.45	Calcarenitic sandstone
MC1	3	Clayey silt
MC2	4.5	Silty shale
MC3	5.2	Silty shale
MC4	7	Clayey silt
MC5	9.35	Silty sand
MC6	11.4	Silty sand
MC7	14	Silty shale
MC8	15.2	Clayey silt
MC9	16.9	Sandstone
MC10	18.5	Calcarenitic sandstone
MC13	25.6	Siltstone

PN samples were collected from borehole Sc1; PR samples from borehole Sc2; and MC samples from borehole Sc3.

CuKα radiation, 45 kV, 35mA, SolX solid-state Si(Li) energy-dispersive detector, measured from 2–70º2θ, 0.02 2θ steps, and 2 s/step count time; (3) a PANalytical X'Pert Pro (PANalytical, Amelo, The Netherlands) at DiSTAR, University of Naples Federico II with measurement conditions of CuKα radiation, 40 kV, 40 mA, RTMS X'Celerator detector, measured from 4–50º2θ, 0.017º2θ equivalent steps, and 60 s/step equivalent time; and (4) a Philips PW1730/3710 (Philips, Eindhoven, The Netherlands) at DiSTAR, University of Naples Federico II with measurement conditions of CuKα radiation, 40 kV, 30 mA, MiniProp detector, measured from 3–35º2θ, 0.02º2θ steps, and 2 s/step count time. PANalytical *HighScore Plus 3.0e* and Bruker AXS *EVA* software were used for mineral identification.

Whole rock XRPD analyses were conducted on samples prepared using the procedures described by Moore and Reynolds (1997). Specifically for the analysis of bulk samples, the material was disaggregated in an agate mortar to obtain a homogeneous powder (particle size <200 μm). Twenty wt.% corundum (α-Al_2O_3, Buehler micropolish, 1 μm grain size) was added for quantitative analyses and this mixture was subsequently micronized (grain size <10 μm) using a McCrone Micronizing Mill (McCrone, Westmont, Illinois, USA) at DiSTAR, University of Naples Federico II with agate cylinders and 10 mL of deionized water for a 15 min grinding time. This technique was used to minimize primary extinction, orientation related problems, and particle statistics problems (Klug and Alexander, 1974; Bish and Chipera, 1987; Srodon *et al.*, 2001).

In order to a) identify clay minerals, b) evaluate the presence of interstratified I-S and C-S, and c) obtain information about the composition and order of interstratified clays, the clay fraction analyses were carried out on oriented mounts of all the samples, except for the calcarenitic materials. The clay fraction was obtained by placing the crushed material in glass blenders and blending with deionized water using a multi-position magnetic stirrer. All suspensions were allowed to settle, then after 24 h the clay fraction in the supernatants was recovered and dried. About 200 mg of the clay fraction was selected and mixed with 1 M $MgCl_2$ solution using a GFL 3005 shaker (GFL Gesellschaft für Labortecknik mbH, Burgwedel, Germany) at DiSTAR, University of Naples Federico II. After Mg saturation (MacEwan and Wilson, 1984), the supernatants were centrifuged for 15 min at 2213 × RCF to sediment the clay. Oriented mounts were prepared using the Moore and Reynolds (1997) smear glass slide method. Ethylene glycol solvation at 60ºC for 8 h was also carried out on the air-dried samples in order to expand clay mineral structures.

The characteristic basal reflections of the clay minerals were analyzed by profile fitting using a Pearson VII function and the *WINFIT* computer program (Krumm, 1996). The number of individual profiles used in this fitting was dictated by the major phases recognized in the qualitative bulk-sample XRPD analysis and in the various treatments of the oriented mounts (Leoni *et al.*, 2010). Chlorite and kaolinite were differentiated by heating the clay fraction as described by Moore and Reynolds (1997).

Quantitative mineral analyses were carried out using the internal standard Rietveld method and Bruker AXS *TOPAS* software. Rietveld refinement alone generally yielded acceptable results when used to evaluate materials that primarily contained three dimensionally ordered materials. For samples that contained poorly ordered phases, such as clay minerals or interstratified phyllosilicates, however, conventional Rietveld refinements without the use of an internal standard did not adequately model the entire diffraction patterns. This led to inaccuracies in mineral quantities and poor information on the quantities of disordered materials, such as the clay minerals. For this reason, the internal standard method was adopted to calculate the total amount of poorly ordered phyllosilicates by difference from 100%. Because the internal standard method allows the absolute (as opposed to the relative) amounts of well-ordered phases to be determined without the constraint that all phases sum to 100%, this approach should provide more accurate results for the well ordered

https://doi.org/10.1346/CCMN.2018.064108 Published online by Cambridge University Press

Table 2. Whole-rock chemical analysis (%) of the major elements as oxides.

	SiO_2	TiO_2	Al_2O_3	Fe_2O_3	MnO	MgO	CaO	Na_2O	K_2O	P_2O_5
PN1	55.70	0.80	16.99	6.92	0.14	5.00	2.40	0.96	0.00	0.11
PN2	50.64	0.74	15.37	6.99	0.10	5.58	5.39	0.91	3.07	0.10
PN3	51.16	0.68	14.71	5.82	0.13	5.06	8.32	1.13	2.91	0.10
PN4	53.57	0.92	16.79	7.52	0.15	3.54	3.94	0.72	3.26	0.11
PN6	53.01	0.87	17.52	6.80	0.09	3.14	4.28	0.91	2.12	0.21
PN6	50.60	0.82	17.94	6.02	0.16	3.85	6.07	1.42	2.66	0.08
PN7	41.67	0.57	13.08	5.81	0.25	3.31	14.77	1.20	2.21	0.10
PN8	50.85	0.77	16.98	6.30	0.13	3.90	6.38	1.29	2.45	0.08
PN9	50.31	0.97	19.45	6.93	0.07	2.83	4.17	0.89	2.51	0.08
PR1	52.23	0.84	16.36	7.00	0.16	3.43	5.28	0.53	3.07	0.16
PR2	50.47	0.77	15.33	6.85	0.16	3.07	7.13	0.62	3.21	0.48
PR3	54.57	0.88	17.57	7.32	0.13	3.75	3.55	0.46	3.51	0.12
PR4	76.74	0.43	4.08	2.69	0.15	1.15	7.17	0.52	0.91	0.01
PR5	58.25	0.43	12.21	3.54	0.06	2.45	10.77	1.24	2.72	0.12
PR6	55.17	0.63	14.43	4.22	0.05	3.17	8.11	0.80	3.53	0.14
PR7	66.76	0.31	13.00	2.53	0.03	1.76	4.84	2.47	2.49	0.08
PR8	49.29	0.79	10.69	6.86	0.18	2.76	6.83	0.74	3.04	0.43
PR9	45.26	0.09	6.61	1.73	0.11	0.91	25.82	1.40	2.17	–
PR10	63.96	0.16	10.49	2.24	0.05	1.37	9.61	1.93	2.83	0.03
PR11	58.51	0.19	9.59	2.18	0.07	1.34	14.54	1.76	2.89	0.03
MC1	52.16	0.96	18.45	7.84	0.23	3.52	4.02	0.46	3.25	0.12
MC2	54.02	0.92	19.51	8.30	0.33	3.42	1.61	0.42	3.55	0.09
MC3	49.93	0.93	18.15	7.59	0.20	3.40	4.43	0.47	3.23	0.12
MC4	54.21	0.92	18.72	7.99	0.21	3.44	1.64	0.40	3.37	0.09
MC5	53.39	0.97	18.98	8.44	0.11	2.95	1.86	0.21	2.01	0.19
MC6	39.84	0.57	12.48	5.10	0.42	2.27	19.94	0.61	2.23	0.04
MC7	43.52	0.51	10.84	4.84	0.34	2.15	18.61	0.44	2.16	0.08
MC8	54.03	0.48	13.10	4.03	0.11	2.03	10.38	1.29	2.78	0.12
MC9	55.41	0.65	14.81	4.95	0.06	2.69	8.83	0.97	3.39	0.13
MC10	60.39	0.54	13.55	4.23	0.07	2.64	6.79	1.08	3.47	0.13
MC11	35.89	0.27	2.53	9.27	1.86	3.37	26.07	0.21	0.06	–
MC12	61.93	0.21	10.59	2.28	0.06	1.18	10.40	2.11	2.86	0.04
MC13	63.21	0.38	14.15	2.80	0.03	1.89	5.92	2.23	3.38	0.10
MC14	60.44	0.28	12.26	2.81	0.05	1.79	9.97	1.89	3.30	0.07

components. Preferred orientation of crystallites was modeled using the March function (Dollase, 1986) and the fundamental parameters approach was used for profiles. The instrumental contribution was modeled along with a Lorentzian crystallite size, a strain component, and a 3rd or 4th order Chebyshev background. Contributions from clay minerals to diffraction patterns were modeled using Pearson VII profiles for the 00l reflections and split Pearson VII profiles to fit the *hkl* bands.

Phyllosilicates with more ordered structures (*e.g.*, muscovite) were directly modeled using the crystal structures. All other clay minerals with partially disordered or disordered structures that do not have three dimensionally ordered structures (interstratified I-S and C-S) were not explicitly included in the refinement (modeled with Pearson VII profiles) and were evaluated by difference from 100%. These XRPD mineralogical results were then used as starting values to determine the amounts of phases using the *vbAffina* software program, which (explained later) recalculates the mineralogy of samples based on the major element chemical composition (whole rock XRF analysis). The following crystal structures were used in the Bruker *TOPAS* software: Na-plagioclase (Harlow and Brown, 1980), maximum microcline (Philips and Ribbie, 1973), 1M biotite (Takeda and Ross, 1975), quartz (Le Page and Donnay, 1976), IIb chlorite (Rule and Bailey, 1987), muscovite (Liang and Hawthorne, 1996), kaolinite (Bish, 1993), and calcite and dolomite (Graf, 1961).

The *vbAffina* program is a Microsoft Visual Basic 6.0 program to quantitatively evaluate the mineralogy of clay rich sediments. It is available free of charge at the website of the Department of Earth Science, University of Pisa. The software, however, is currently unavailable because the authors are improving it as well as translating it into English to facilitate international distribution. The *vbAffina* program estimates the relative amounts of different mineral phases by combining chemical analyses (*e.g.*, XRF data) and XRPD quantitative mineralogical data (Leoni *et al.*, 1989, 2008). It requires as input data: a) qualitative identification and a quantitative estimate of the mineral phases in the sample obtained by XRPD methods; b) the major element

https://doi.org/10.1346/CCMN.2018.064108 Published online by Cambridge University Press

composition of the bulk sample (in this case, SiO_2, Al_2O_3, Fe_2O_3, MgO, CaO, Na_2O, and K_2O); c) the amounts of CO_2 and H_2O^+, or $CO_2 + H_2O^+$ as LOI; and d) estimates of the chemical compositions of individual minerals in the samples. The data were processed using a least squares procedure that minimizes the differences between chemical compositions calculated from the XRD-determined phase percentages that were introduced into *vbAffina* (*i.e.*, XRPD results) and those determined using XRF (Leoni *et al.*, 2008). The system also allows the amount of some phases, such as calcite and/or dolomite, to be constrained based on independent estimates (*e.g.*, from CO_2 analyses). Other constraints include the allowed range for each different phase analyzed. During the calculation, the software can incrementally vary the percentages of all the phases by 0.5% or 1% (and so on in 0.5% steps). The software then automatically calibrates the most statistically representative values of the mineral phases and, thereby, determines a Gaussian distribution with the most likely percent value for a given phase.

Stoichiometric compositions of quartz, calcite, dolomite, Na-plagioclase (albite), microcline (orthoclase in *vbAffina*), and kaolinite were used with *vbAffina* (Table 3). The initial chlorite, muscovite/illite, and smectite compositions were selected from a *vbAffina* database that contained the compositions of these minerals. The software automatically calculates both the amount of each phase and the chemical composition of individual components for each sample. For the analyses in the present study, dioctahedral smectite was assumed to be the smectitic portion of interstratified I-S based on XRPD analysis, and trioctahedral smectite was used to represent the smectitic portion of interstratified C-S. These assumptions were justified by the fact that the normal transition from smectite to illite involves dioctahedral smectite, whereas trioctahedral smectite usually transforms to chlorite (Meunier *et al.*, 1991; Son *et al.*, 2001). After calculating chlorite, illite, and smectite quantitites as discrete phases, interstratified I-S and C-S were estimated based on the ratio of end members according to Moore and Reynolds (1997) and by assuming the percent smectite that was calculated based on the chemical composition.

RESULTS

Qualitative XRPD Analyses

Results revealed that the use of different methods for sample preparation and different instruments did not influence the final results, and comparisons of the data from DiSTAR, CNR, and Indiana University closely agreed. Qualitative XRPD analyses showed that the samples contained phyllosilicate minerals (chlorite, kaolinite, illite-muscovite, and interstratified I-S and C-S), quartz, feldspars (Na-plagioclase and microcline), and carbonate minerals (calcite and dolomite) (Figure 3). Interstratified C-S was not obvious in the bulk sample XRPD patterns because of the peak overlap between chlorite and mixed-layer I-S, which was only revealed by XRD patterns of glycolated oriented mounts (Figure 5).

In detail, all samples from the Sc1 core (Figure 1, Table 1) were characterized by the presence of quartz, feldspars, and calcite, but dolomite content was generally low (Figure 3a). Chlorite and illite-muscovite were also present, but discrete kaolinite was detected only in samples PN4, PN5, PN6, PN8, and PN9. Interstratified I-S was present in all samples (Figure 3a and Table 4). Both R0 and R1 Reichweite values for I-S were characteristic of samples PN2, PN4, and PN6 to PN9. Sample PN1 contained I-S with R1 and R3 Reichweite values (Table 4) and the I-S in samples PN3 and RN5 had R1 and R0 values, respectively (Table 4). Interstratified C-S with an R0 value was present in all samples, except PN5 and PN8 (Table 4).

Samples from core Sc2 (Figure 1, Table 1) were characterized mainly by quartz, feldspars, and calcite

Table 3. Chemical composition of minerals used in the vbAffina (wt.%).

	CO_2	Na_2O	MgO	Al_2O_3	SiO_2	K_2O	CaO	FeO
Quartz	0	0	0	0	100	0	0	0
Calcite	44	0	0	0	0	0	56	0
Dolomite	48	0	22	0	0	0	30	0
Albite	0	12	0	19	69	0	0	0
Anortite	0	0	0	37	43	0	20	0
Ortose	0	0	0	18	65	17	0	0
Kaolinite	0	0	0	46.5	c	0	0	0
Illite	0	0	3.2	30.2	56.4	10.2	0	0
Chlorite	0	0	17.9	18.2	32	0	0	31.9
Smectite D	0	0	2.9	24.9	70.3	0	0	1.9
Smectite T	0	0	23.8	4.4	57.7	0	0	14.1

Smectite D = dioctahedral smectite; Smectite T = trioctahedral smectite.
Further information about the chemical composition of minerals are reported by Leoni *et al.* (1989).

https://doi.org/10.1346/CCMN.2018.064108 Published online by Cambridge University Press

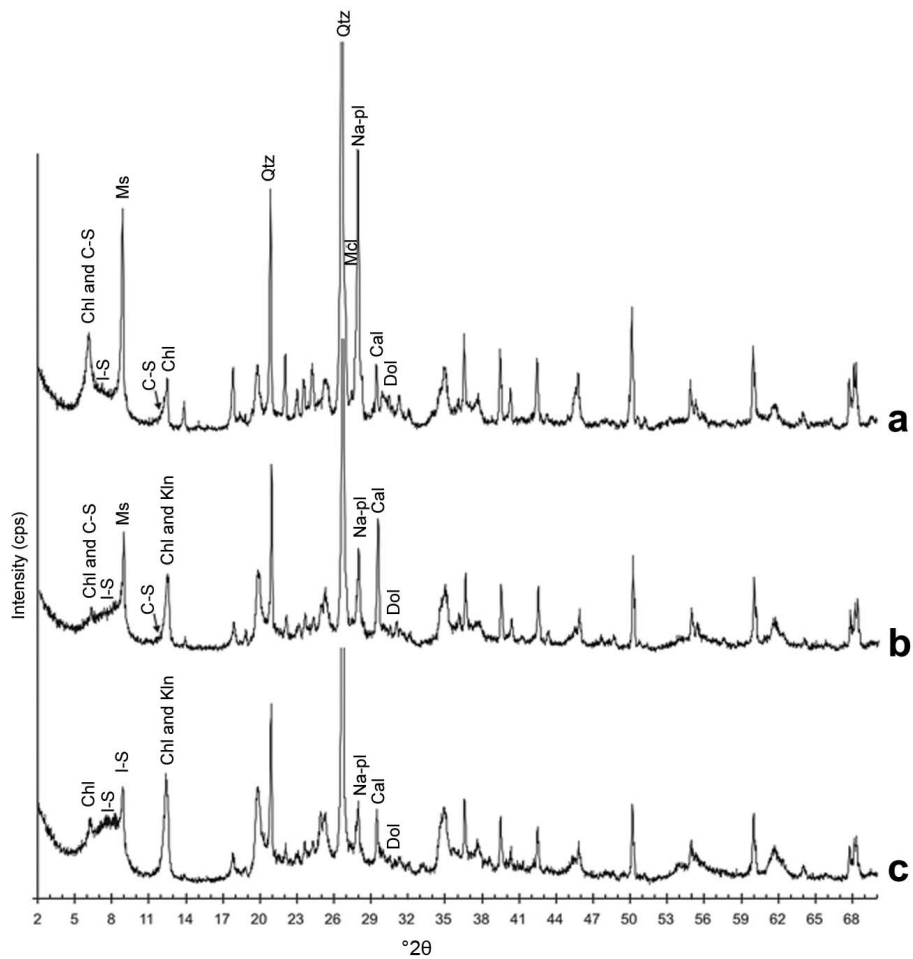

Figure 3. Representative XRPD patterns of samples from borehole (a) Sc1-PN1 sample; (b) Sc2-PR1 sample; (c) Sc3-MC2 sample. Chl = chlorite; I-S = interstratified illite-smectite; C-S = interstratified chlorite-smectite; Kln = kaolinite; Ms = muscovite; Qtz = quartz; Mcl = microcline; Na-pl = Na-plagioclase; Cal = calcite; Dol = dolomite.

(Figure 3b). Illite and/or mica with 10 Å peaks and 14 Å chlorite peaks were pronounced in the XRPD patterns as well as the characteristic broad low-angle diffraction features of interstratified I-S (Figure 3b). Both R0 and R1-ordered I-S were present in PR1, PR2, PR3, and PR5 (Table 4), whereas samples PR6 and PR7 were characterized by the presence of only R1-ordered I-S (Table 4). R0 interstratified C-S was detected in samples PR1, PR2, and PR3 (Table 4). Kaolinite was detected in only the four PR1, PR2, PR3, and PR6 samples.

Samples from the Sc3 core (Figure 1, Table 1) were characterized by quartz, Na-feldspar, K-feldspar, and calcite (Figure 3c). In addition, heating tests on the oriented mounts confirmed kaolinite in all samples, except for samples MC8, MC9, and MC10. Chlorite, a 10 Å phase (illite-muscovite), and interstratified I-S were identified in all Sc3 samples. In detail, MC1 and samples from MC6 to MC10 had both R0 and R1-ordered interstratified I-S (Table 4). R1-ordered interstratified I-S was detected in samples MC2, MC3, MC4, MC6, MC7, MC8, MC9, MC10, and MC13 (Table 4). R0 interstratified C-S was present in all samples except MC2, MC3, MC4, and MC13 (Table 4).

Quantitative analyses

Internal-standard Rietveld analyses. Quantitative mineralogical data obtained using Bruker *TOPAS* software (Table 5) did not provide the amount of any interstratified C-S independently from interstratified I-S because interstratified C-S was not obvious in the bulk sample XRPD patterns (Figure 4). The total amounts of interstratified clay minerals (I-S + C-S) were always calculated by difference from 100% using the internal standard method. As shown in Table 5, all samples were dominated by I-S and C-S with lesser amounts of kaolinite, chlorite, muscovite, quartz, Na and K-feldspars, calcite, and traces of dolomite.

vbAffina analysis. Mixed-layer I-S was modeled with the *vbAffina* program using the amounts of illitic and

https://doi.org/10.1346/CCMN.2018.064108 Published online by Cambridge University Press

Table 4. Percentage of illitic and chloritic layers in interstratified I-S and C-S, respectively, and associated Reichweite values.

ID sample	I-S		C-S	
	Reichweite value	% Illitic layers	Reichweite value	% Chloritic layers
PN1	R1; R3	63; 82	R0	50
PN2	R0; R1	37; 76	R0	50
PN3	R1	71	R0	40
PN4	R0; R1	28; 77	R0	50
PN5	R0	56	–	–
PN6	R0; R1	28; 74	R0	55
PN7	R0; R1	45; 76	R0	57
PN8	R0; R1	38; 80	–	–
PN9	R0; R1	34; 77	R0	42
PR1	R0; R1	59; 67	R0	53
PR2	R0; R1	35; 67	R0	38
PR3	R0; R1	45; 82	R0	43
PR5	R0; R1	45; 74	–	–
PR6	R1	76	–	–
PR7	R1	74	–	–
MC1	R0; R1	60; 74	R0	55
MC2	R1	76	R0	55
MC3	R1	74	–	–
MC4	R1	75	R0	52
MC5	R0	49	–	–
MC6	R0; R1	45; 67	–	–
MC7	R0; R1	30; 76	–	–
MC8	R0; R1	24; 75	R0	55
MC9	R0; R1	36; 76	R0	65
MC10	R0; R1	35; 73	R0	60
MC13	R1	76	R0	40

Table 5. XRPD quantitative results (wt.%) from internal-standard Rietveld refinement.

ID sample	I-S+C-S	Ms	Kln	Chl	Qz	Mcl	Na-pl	Cal	Dol
PN1	31	16	–	3	26	4	15	5	<1
PN2	31	17	–	2	22	4	12	10	1
PN3	24	16	–	2	28	4	16	9	2
PN4	59	5	–	3	18	4	6	4	1
PN5	50	3	3	3	22	6	4	8	<1
PN6	49	7	1	7	17	4	7	6	5
PN7	39	3	–	7	16	3	7	21	3
PN8	39	5	–	5	23	3	9	10	5
PN9	61	3	5	2	16	3	3	5	1
PR1	52	6	–	3	19	6	8	6	<1
PR2	54	6	5	6	15	6	6	7	1
PR3	46	10	–	3	21	7	7	6	<1
PR5	18	8	–	2	34	8	15	14	1
PR6	46	1	–	4	23	8	11	6	–
PR7	14	5	–	3	45	8	21	5	<1
MC1	63	5	–	1	17	5	5	3	<1
MC2	65	6	1	3	16	3	4	3	1
MC3	55	5	4	6	16	7	4	4	1
MC4	55	7	1	3	21	4	4	4	<1
MC5	61	3	5	6	19	2	1	3	<1
MC6	18	4	1	2	22	6	7	39	1
MC7	36	2	<1	5	27	7	12	9	1
MC8	13	6	–	<1	28	5	12	33	2
MC9	38	2	4	4	25	7	10	8	1
MC10	37	2	4	3	29	8	12	6	<1
MC13	45	6	–	2	30	6	5	4	2

I-S+C-S = mixed-layers; Ms = muscovite; Na-pl = Na-plagiocase; Qz = quartz; Cal = calcite; Chl = chlorite; Kln = kaolinite; Mcl = microcline; Dol = dolomite; – = not detected.

https://doi.org/10.1346/CCMN.2018.064108 Published online by Cambridge University Press

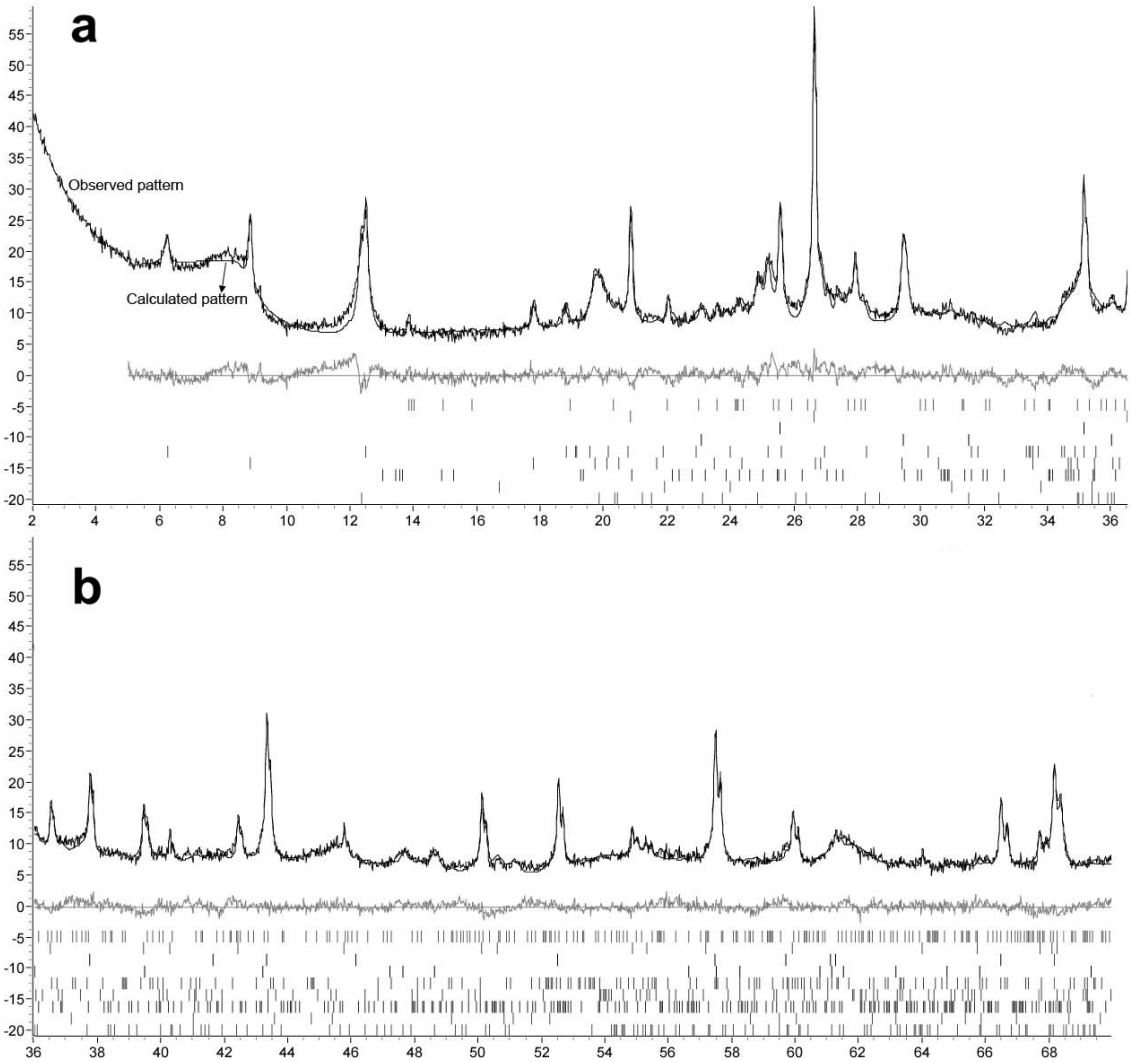

Figure 4. Results of Rietveld refinement using *TOPAS* for sample PN4 Gray line at a y-axis value of zero represents the difference between observed and calculated profiles, and the small vertical tic marks at the bottom of the plot represent the positions of all possible reflections for each phase. (a) 2−36º2θ, (b) 36−70º2θ.

smectitic layers from the XRPD-determined amount of the illitic component in interstratified I-S. Figure 5 contains representative XRPD patterns of sample clay fractions that are characterized by: illite, chlorite, and R0 interstratified I-S (Figure 5a); illite, chlorite, R0 and R1-ordered I-S, and R0 C-S (Figure 5b); illite, chlorite, and R0 I-S (Figure 5c); and illite, chlorite, R1- and R3-ordered I-S, and R0 C-S (Figure 5d). The degree of order in interstratified I-S was determined using the peak position between 5 and 8.5º2θ (CuKα radiation) (Moore and Reynolds, 1997). In detail, the R0 I-S was characterized by a peak at ~5.3º2θ (Figures 5a and 5b). The R1-ordered I-S has a peak from 6.5 to 7.5º2θ (Figures 5b and 5c) and the R3-ordered I-S has a peak between 8.0 and 8.5º2θ (Figure 5d). Interstratified I-S was the primary clay mineral and the content ranged from 15 to 52 wt.% in all the samples (Table 6). Because interstratified C-S was only identified in XRPD patterns

Figure 5 (*facing page*). Representative XRPD patterns of oriented ethylene glycol-solvated aggregates characterized by the presence of: (a) R0 interstratified I-S, MC5 sample; (b) R0 and R1 interstratified I-S, PR2 sample; (c) R1 interstratified I-S, PR7 sample; (d) R1 and R3 interstratified I-S and R0 interstratified C-S, PN1 sample. I-S = interstratified illite-smectite; C-S = interstratified chlorite-smectite; Chl = chlorite; Ill = illite; Kln = kaolinite; Qtz = quartz; Na-pl = Na-plagioclase. Higher-angle portions of the XRPD patterns have been scaled up in intensity in comparison with the low-angle portions.

https://doi.org/10.1346/CCMN.2018.064108 Published online by Cambridge University Press

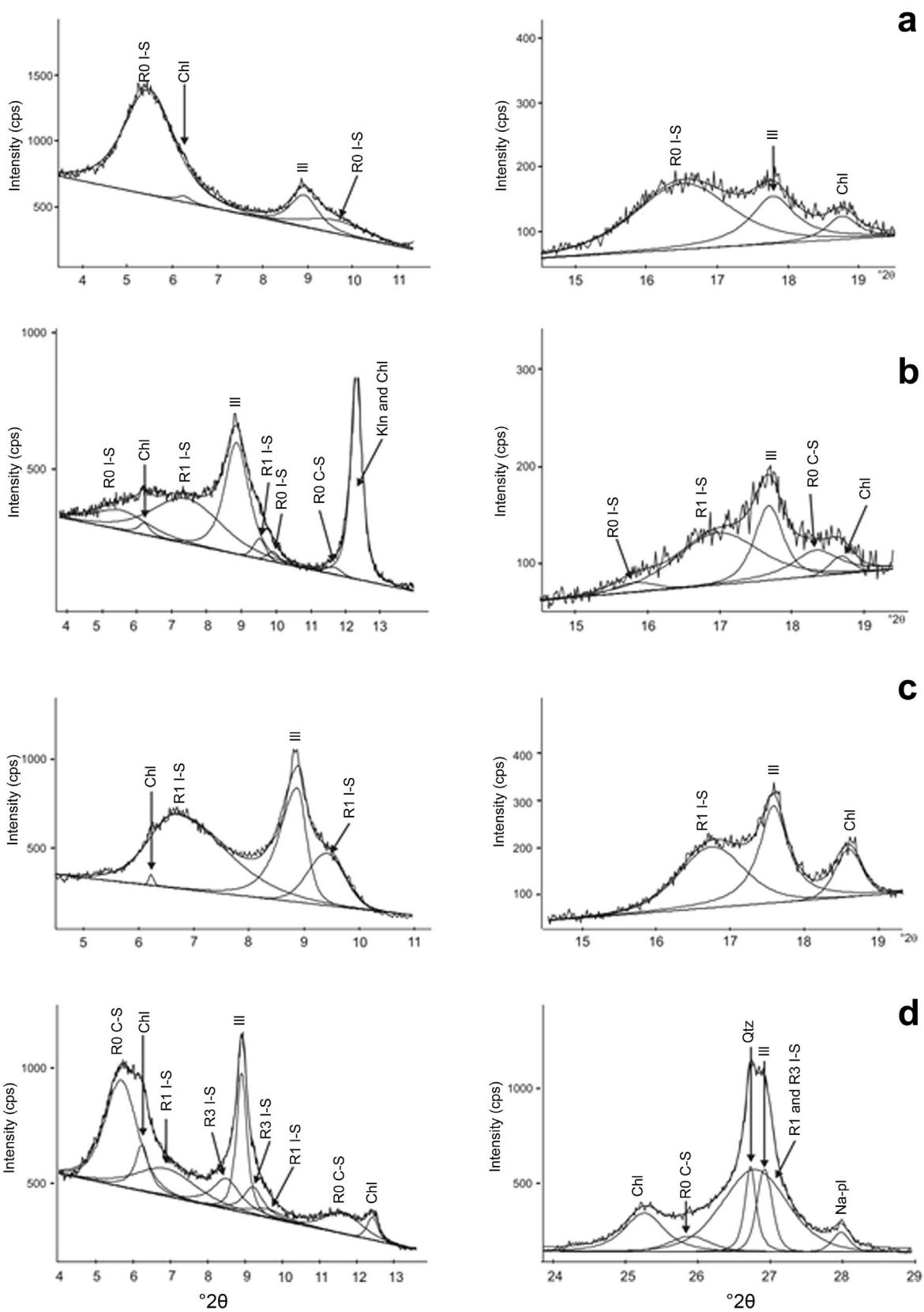

https://doi.org/10.1346/CCMN.2018.064108 Published online by Cambridge University Press

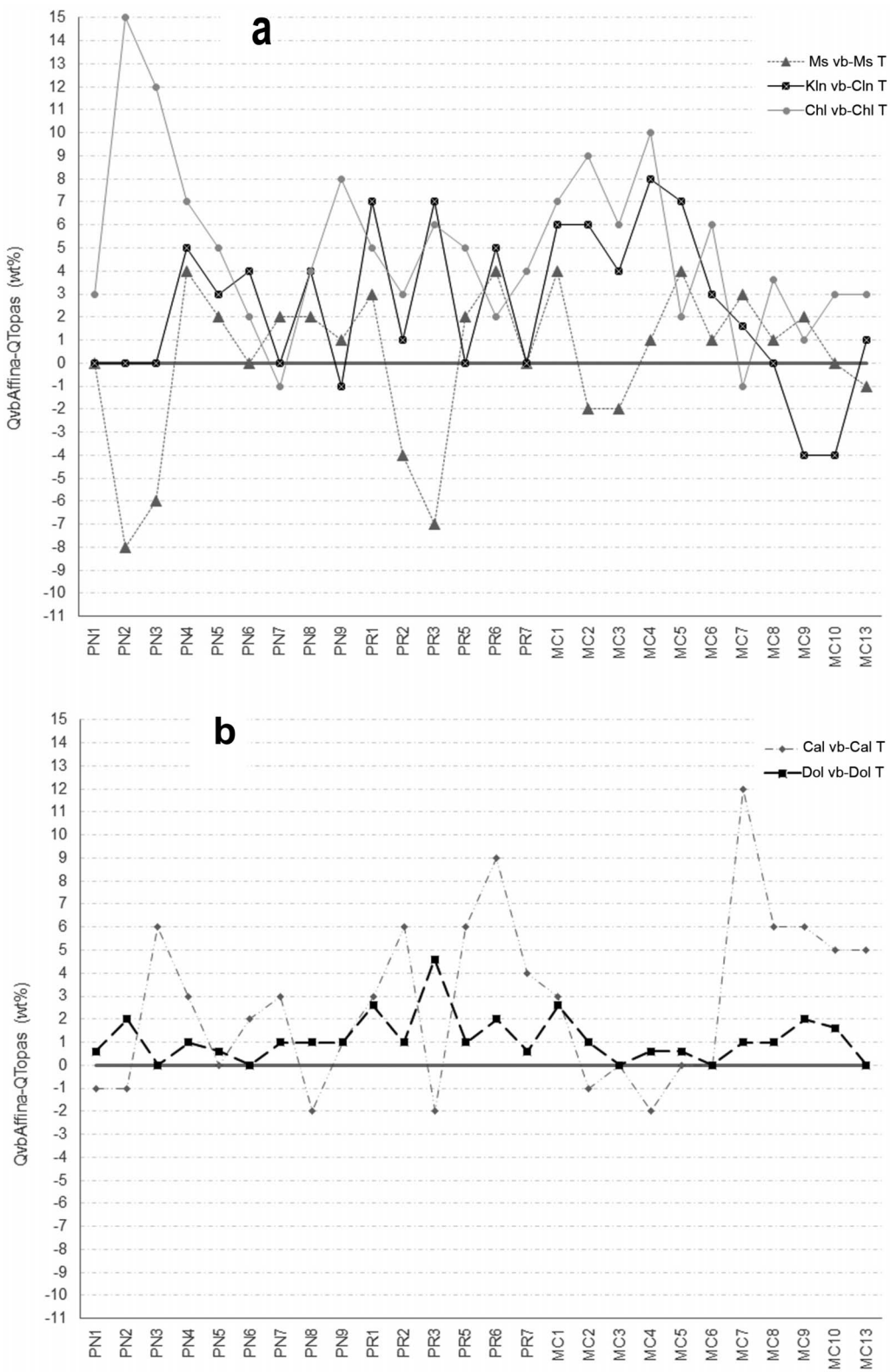

Figure 6. Differences between quantitative analyses obtained using Bruker *TOPAS* and *vbAffina* software: (a) Ms vb-Ms T, Kln vb-Cln T, and Chl vb-Chl T mineral phases; (b) Cal vb-Cal T and Dol vb-Dol T mineral phases.

https://doi.org/10.1346/CCMN.2018.064108 Published online by Cambridge University Press

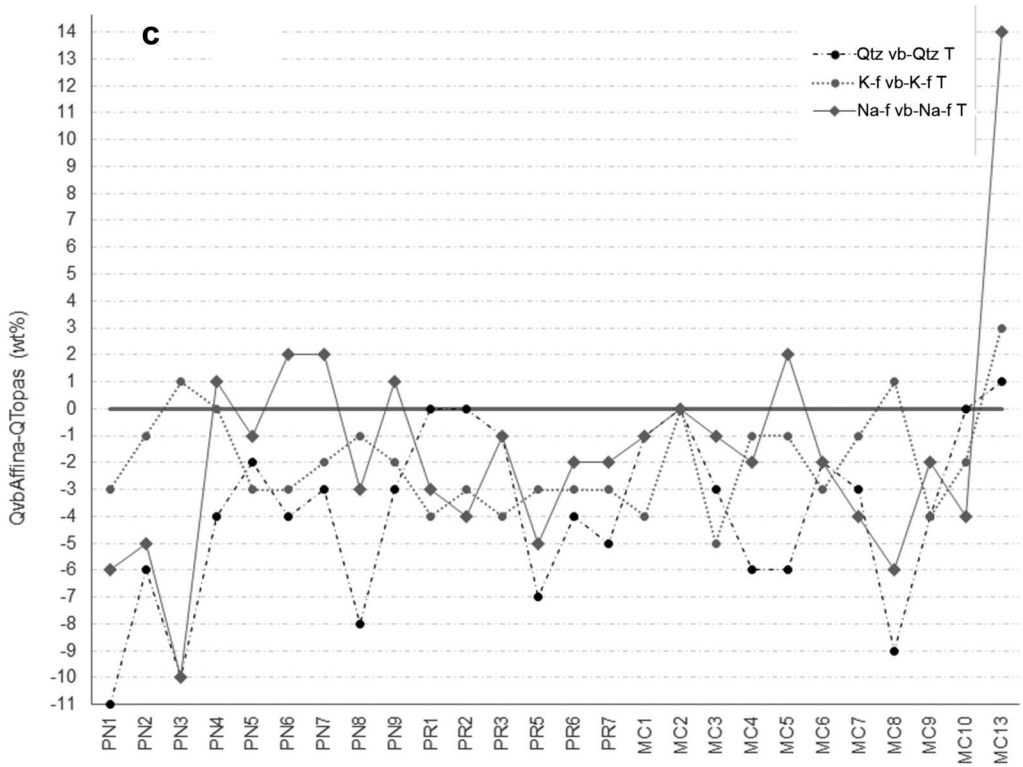

Figure 6 (*contd.*). (c) Qtz vb-Qtz T, K-f vb-K-f T, and Na-f vb-Na-f T mineral phases.

of oriented aggregates, an initial content of 4−5 wt.% interstratified C-S, which contained various amounts of trioctahedral smectite and chlorite, was estimated based on visual observations of the patterns. The *vbAffina* refined C-S content did not change significantly from the input values and typically remained within the estimated error of ±1 wt.%. The refined C-S content was only significantly greater than the average C-S values for sample PN1 (Table 5), which yielded 15 wt.% interstratified C-S. The diagnostic corrensite reflection at about 11.4º2θ in the XRPD pattern of the glycolated material was used to determine the degree of ordering of the interstratified C-S (Moore and Reynolds, 1997).

A comparison between Table 5 and Table 6 revealed the differences between the results obtained by the two different methods. The internal standard Rietveld method provided information on individual crystalline phases and on the sum of the unmodeled phases (*i.e.*, clay mineral phases, interstratified I-S and C-S). The single value for the total clay mineral phases obtained by difference by this method (Table 5) was commonly lower than the sum of the interstratified I-S and C-S contents calculated using *vbAffina*. Because this discrepancy is associated with decreased amounts of quartz and feldspars determined using *vbAffina* in comparison with the amounts determined using the internal standard Rietveld method, the *vbAffina* likely recalculated the phyllosilicate content and subtracted the Si that was originally assigned to quartz and feldspar. Figures 6b and 6c show that the Na-plagioclase, quartz, microcline, calcite, muscovite, and kaolinite contents that were evaluated by *TOPAS* in sample MC13 are lower than the values determined using *vbAffina* (Figure 6a). The amount of interstratified I-S calculated using *vbAffina* was significantly lower (17 wt.%) than the amount obtained by difference using Rietveld refinement (45 wt.%) (Table 6). The amount of interstratified I-S determined by *vbAffina* provided better agreement between measured and calculated bulk chemistry.

DISCUSSION

Quantitative evaluation of clay-rich sediments

Quantitative mineralogical analyses of the clay-rich sediments employed a combination of methods to accommodate the presence of disordered phyllosilicates, such as interstratified minerals. Such minerals are characterized by a variable chemical composition and degree of order and both strongly influence the diffracted intensities and the ability to model XRPD data. In the present study, two interstratified phases (I-S and C-S) were identified and evaluated independently using ethylene glycol solvated samples. The I-S was clearly recognized in bulk-sample XRPD patterns and with oriented aggregates, whereas the C-S was apparent only in the oriented mount patterns of most materials. Because the conventional Rietveld method is not capable of accurately modeling disordered (*e.g.*, interstratified I-

https://doi.org/10.1346/CCMN.2018.064108 Published online by Cambridge University Press

Table 6. Results (wt.%) of combined XRD/XRF analysis using *vbAffina.*

ID sample	I-S	C-S	Ms	Kln	Chl	Qtz	Mcl	Na-pl	Cal	Dol
PN1	33	15	16	–	6	15	1	9	4	1
PN2	36	–	9	–	17	16	3	7	9	3
PN3	26	4	10	–	14	18	5	6	15	2
PN4	38	4	9	5	10	14	4	7	7	2
PN5	47	–	5	6	8	20	3	3	8	1
PN6	39	4	7	5	9	13	1	9	8	5
PN7	34	4	5	–	6	13	1	9	24	4
PN8	43	–	7	4	9	15	2	6	8	6
PN9	52	4	4	4	10	13	1	4	6	2
PR1	34	4	9	7	8	19	2	5	9	3
PR2	44	4	2	6	9	15	3	2	13	2
PR3	39	4	3	7	9	20	3	6	4	5
PR5	19	–	10	–	7	27	5	10	20	2
PR6	34	–	5	5	6	19	5	9	15	2
PR7	14	–	5	–	7	40	5	19	9	1
MC1	43	4	9	6	8	16	1	4	6	3
MC2	46	4	4	7	12	16	3	4	2	2
MC3	54	–	3	8	12	13	2	3	4	1
MC4	43	4	8	9	13	15	3	2	2	1
MC5	52	–	7	12	8	13	1	3	3	1
MC6	15	–	5	4	8	20	3	5	39	1
MC7	28	–	5	2	4	24	6	8	21	2
MC8	12	4	7	–	4	19	6	6	39	3
MC9	38	4	4	–	5	21	3	8	14	3
MC10	32	4	2	–	6	29	6	8	11	2
MC13	17	2	5	1	5	31	9	19	9	2

I-S = mixed-layer illite-smectite; C-S = mixed-layer chlorite-smectite; Ms = muscovite; Na-pl = Na-plagiocase; Qz = quartz; Cal = calcite; Chl = chlorite; Kln = kaolinite; Mcl = microcline; Dol = dolomite; - = not detected.
*sum of the squares of the differences between the XRF chemical analyses and the chemistry implied by the mineral wt.% data obtained through *vbAffina.*

S and C-S) and poorly ordered materials, the amounts of these components can be evaluated by difference from 100% using the internal standard Rietveld method. In the studied samples, no diffraction evidence appeared for poorly ordered materials other than clay minerals and the internal standard Rietveld method was only used to evaluate the amounts of interstratified I-S and C-S. In order to refine the mineralogical results, the *vbAffina* software was used to calculate the amounts of mineral phases and calibrated the XRPD determined values using the bulk chemical data for whole samples and the chemical compositions of individual minerals. The *vbAffina* program was used to determine the amounts of individual interstratified minerals, which were not determined after Rietveld refinement. Although the chemical compositions of several minerals (*e.g.*, quartz, microcline, kaolinite, calcite) are approximately constant, other phases (*e.g.*, interstratified clays, chlorite, Na-plagioclase, illite) are generally characterized by a variable composition that is more difficult to constrain and, thereby, influences the quality of the results. In this case, the differences in the results were likely affected by inaccuracies in the chemical compositions of individual phases (*e.g.*, chlorite, plagioclase, illite) and by the effects of disordered phases on the diffraction patterns (Tables 5 and 6 and Figure 6). Because the amounts of clay minerals were determined by difference from 100% using the internal standard method with *TOPAS*, any errors in modeling the non-clay portion of a sample will affect the quantification of all components. Thus, chemical data were used together with *TOPAS* results to increase the accuracy of the mineralogical quantifications of all phases. Although no amorphous material was detected in the XRPD patterns, small amounts of such materials could be present and would contribute to small inaccuracies in the final mineral quantifications (*e.g.*, Bish and Chipera, 1987).

Evaluation of mineralogy effects on landslide development

The mineralogy of the materials involved in the landslide (obtained in the present study) in comparison with the petrography of the "undisturbed" rocks that constitute the *Arenarie di Termini* Formation (reported in Iannace *et al.*, 2015) illustrate that the landslide materials are clay-rich rocks characterized by abundant interstratified I-S. The I-S is associated in several samples with interstratified C-S, which can be considered as products of *in situ* weathering. Relatively minor amounts of quartz, feldspar, and calcite with traces of

https://doi.org/10.1346/CCMN.2018.064108 Published online by Cambridge University Press

dolomite were also present. The rocks of the *Arenarie di Termini* Formation that were not involved in the landslide resemble quartz-feldspar sandstones and are characterized by abundant detrital quartz, feldspar, and minor amounts of lithic components (plutonic, gneiss, slate, phyllite, *etc*.) with few clay minerals (Iannace *et al.*, 2015). The differences between the mineral suites of the studied *Arenarie di Termini* Formation sandstones are noteworthy because the materials involved in the landslide contain greater amounts of clay minerals than the "undisturbed" original rocks. Results suggest that the abundant clays that occur in the landslide material were produced by *in situ* weathering of the *Arenarie di Termini* Formation. Although interstratified I-S clays in other areas of the southern Apennines have not been considered to be products of *in situ* weathering but as products of diagenetic processes that occurred during consolidation and burial (as described for example by Cavalcante *et al.*, 2007), the widespread presence of R0 interstratified I-S noted in the present study suggests that at least a portion of the studied materials are genetically related to surficial weathering processes. The R1- and R3-ordered interstratified I-S clays, which are generally associated with a greater degree of diagenesis, are likely the residual products of ancient parent rocks that occur here in the lithic component of the arkose. The C-S interstratified clays are commonly associated with volcanoclastic sediments or various types of altered igneous rocks, as well as ancient marine evaporites, carbonates, or lacustrine facies, but can also be produced by weathering of chlorite *sensu strictu* (Hillier, 1993). Iannace *et al.* (2015) reported the occurrence of lithic fragments of clear igneous origin, as well as gneiss, slate, and phyllite with rare serpentinite, siltstone, and shale fragments in the unweathered *Arenarie di Termini* Formation. Thus, the lithic component of the analyzed material may contain C-S, where it is related to an ancient diagenetic or low-temperature metamorphic event(s) as in the R1- and R3-ordered interstratified I-S or it is a product of chlorite weathering. Irrespective of these details, the landslide is located in the weathered realm that overlies the quartz-feldspar-bearing siliciclastic rocks of the *Arenarie di Termini* Formation.

Physical chemical weathering processes are generally assumed to promote the formation of alteration zones in soil horizons, which are characterized by different types of clay minerals (Taylor and Spears, 1970; Taylor and Cripps, 1987; Velde, 1995). In the studied Termini Nerano area, however, the amount of smectitic layers in interstratified I-S was not regularly distributed along vertical sections of soil horizons. The absence of soil alteration zones or of a regular distribution of smectite with depth can be explained by invoking intense reworking of the soil that is related to the landslide or, alternatively, by preferential soil alteration along joints and discontinuities of the rock which led to the formation of "imperfect" weathering zones.

CONCLUSIONS

This study reports the results of a detailed study of the mineralogy of heterogeneous clay-bearing rocks involved in a landslide in the *Arenarie di Termini* Formation. These rocks contain several phyllosilicates (chlorite, kaolinite, interstratified I-S and C-S, and muscovite) and carbonates, quartz, and feldspars. The internal standard Rietveld method was used to determine the mineralogy of the "crystalline" (*i.e.*, non-clay portion) components, but this method provided information only on the sum of all the disordered components by difference (*e.g.*, interstratified I-S and C-S). The combination of these mineralogical data with chemical data allowed quantification of all the phases that comprise the selected material.

The mineralogy of the material involved in the landslide (Table 6) in comparison with the rocks that were not involved in the landslide (Iannace *et al.*, 2015) showed that the landslide was perfectly located in the weathered realm that overlies the quartz-feldspar-bearing siliciclastic rocks of the *Arenarie di Termini* Formation. The material involved in the landslide is characterized by minerals related to more surficial weathering-related processes (*e.g.*, R0 interstratified I-S and possibly also C-S) and also by minerals genetically related to diagenetic or metamorphic processes that were inherited from the *Arenarie di Termini* Formation (*e.g.*, chlorite, kaolinite, R1- and R3-ordered interstratified I-S and C-S, muscovite, quartz, and feldspars).

ACKNOWLEDGMENTS

M. Cesarano and co-authors are grateful to the anonymous reviewers and associate editor for their comments and criticism that helped to improve this contribution. The authors would also like to thank the IDROGEO srl company that carried out borehole drilling in the studied area. The project received funding from *Progetto FARO* (CUP E61J1100026000; Prot. N. 2012/0066340 - 15/06/2012.

REFERENCES

Bianconi, G. (1840) *Storia Naturale dei Terreni Ardenti, dei Vulcani Fangosi, delle Sorgenti Infiammabili, dei Pozzi Idropirici e di Altri Fenomeni Geologici Operati dal Gas Idrogene e dalla Origine di Esso Gas*. Marsigli, Bologna, 164 pp.

Bish, D.L. (1993) Rietveld refinement of the kaolinite structure at 1.5 K. *Clays and Clay Minerals* **41**, 738–744.

Bish, D.L. and Chipera, S.J. (1987) Problems and solution in quantitative analysis of complex mixture by X-ray powder diffraction. *Advances in X-ray Analysis*, **31**, 295–307.

Bish, D.L. and Howard, S.A. (1988) Quantitative phase analysis using the Rietveld technique. *Journal of Applied Crystallography*, **21**, 86–91.

Brindley, G.W. (1980) Quantitative X-ray mineral analysis of clays. Chapter 7, pp. 411–438 in: *Crystal Structures of Clay Minerals and their X-ray Identification* (G.W. Brindley and G. Brown, editors). Monograph 5. Mineralogical Society,

https://doi.org/10.1346/CCMN.2018.064108 Published online by Cambridge University Press

London.
Calcaterra, D., Croce, C., de Luca Tupputi Schinosa, F., Di Martire, D., Parise, P., Ramondini, M., Borrelli, E., Salzano, M., and Serricchio, A. (2006) The Colle Lapponi-Piano Ovetta landslide (Agnone, Molise, Italy), an example of rainfall-induced reactivation in weathered structurally complex materials. *Geophysical Research Abstracts*, **8**. European Geosciences Union.
Calcaterra, D., Cal, F., Cappelletti, P., de'Gennaro, M., Di Martire, D., Parise, M., and Ramondini, M. (2007) Mineralogical and geotechnical characterization of large earthflow in weathered structurally complex terrains of the Molise region, Italy. *Geophysical Research Abstracts.*
Calvert, C.S., Palkovsky, D.A., and Pevear, D.R. (1989) A combined X-ray powder diffraction and chemical method for the quantitative mineral analysis of geologic samples.pp. 154–166 in: *Quantitative Mineral Analysis of Clays* (D.R. Pevear and F.A. Mumpton, editors). CMS Workshop Lectures 1. The Clay Minerals Society, Boulder, Colorado, USA.
Cascini, L., Bonnard, C., Corominas, J., Jibson, R., and Montero-Olarte, J. (2005) Landslide hazard and risk zoning for urban planning and development. State of the art report. *Proceedings of the International Conference on Landslide Risk Management*. Taylor and Francis, London, 199–235.
Cavalcante, F., Fiore, S., Lettino, A., Piccarreta, G., and Tateo, F. (2007) Illite-smectite in sicilic shales and piggy-back deposits of the Gorgoglione Formation (Southern Apennines): Geological Inferences. *Italian Journal of Geoscience*, **126**, 241–254.
Chipera, S.J. and Bish, D.L. (2002) FULLPAT: A full-pattern quantitative analysis program for X-ray powder diffraction using measured and calculated patterns. *Journal of Applied Crystallography*, **35**, 744–749. doi:10.1107/S0021889802017405.
Cotecchia, V. and Melidoro, G. (1966) Geologia e frana di Termini Nerano (Penisola Sorrentina). *Geologia Applicata e Idrogeologia*, **1**, 93–126.
Cruden, D.M. and Varnes, D.J. (1996) Landslides types and processes. Pp. 36–75 in: *Landslides: Investigation and Mitigation* (A.K. Turner, R.J. Schuster, editors), Special Report 247 pp. Transportation Research Board, National Academy Press, Washington, DC.
De Ruan, C. and Ward, C.R. (2002) Quantitative X-ray powder diffraction analysis of clay minerals in Australia coals using Rietveld methods. *Applied Clay Science*, **21**, 227–240.
Di Bucci, D., Parotto, M., Adatte, T., Gianpaolo, C., and Kubler, B. (1996) Mineralogia delle argille varicolori dell'Appennino centrale: Risultati preliminari e prospettive di ricerca. *Bollettino della Società Geologica Italiana*, **115**, 689–700.
Dollase, W.A. (1986) Correction of intensities for preferred orientation in powder diffractometry: Application of the March model. *Journal of Applied Crystallography*, **19**, 267–272.
Dumon, M., Tolossa, A.R., Capon, B., Detavernier, C., and Van Ranst, E. (2014) Quantitative clay mineralogy of a Vertic Planosol in southwestern Ethiopia: Impact on soil formation hypotheses. *Geoderma*, **214–215**, 184–196.
Graf, D.L. (1961) Crystallographic tables for the rhombohedral carbonates. *American Mineralogist*, **46**, 1283–1316.
Harlow, G.E. and Brown, G.E. (1980) Low albite: An X-ray and neutron diffraction study. *American Mineralogist*, **65**, 986–995.
Hillier, S. (1993) Origin, diagenesis and mineralogy of chlorite in Devonian lacustrine mudrocks, Orcadian basin, Scotland. *Clays and Clay Minerals*, **41**, 240–259.
Iannace, A., Merola, D., Perrone, V., Amato, A., and Cinque, A. (2015) Note illustrative della carta geologica d'Italia alla scala 1:50.000 Foglio 466–485 Sorrento-Termini. *Servizio Geologico d'Italia*, ISPRA, 204 pp.
Klug, H.P. and Alexander, L.E. (1974) *X-ray Diffraction Procedures for Polycrystalline and Amorphous Materials*. J. Wiley and Sons, New York, 992 pp.
Le Page, Y. and Donnay, G. (1976) Refinement of the crystal structure of low-quartz. *Acta Crystallographica*, section B **32**, 2456–2459.
Leoni, L., Saitta, M., and Sartori, F. (1989) Analisi mineralogica quantitative di rocce e sedimenti pelitici mediante combinazione di dati diffrattometrici e chimici. *Rendiconti della Società Geologica Italiana di Mineralogia e Petrografia*, **43**, 743–756.
Leoni, L., Lezzerini, M., and Saitta, M. (2008) Calcolo computerizzato dell'analisi mineralogica quantitativa di rocce e sedimenti argillosi basato sulla combinazione dei dati chimici e diffrattometrici. *Atti della Società Toscana de Scienze Naturali di Pisa*, Serie A, **113**, 63–69.
Leoni, L., Lezzerini, M., Battaglia, S., and Cavalcante, F. (2010) Corrensite and chlorite-rich Chl-S mixed layers in sandstones from the 'Macigno' Formation (northwestern Tuscany, Italy). *Clay Minerals*, **45**, 87–106.
Liang, J. and Hawthorne, F.C. (1996) Rietveld refinement of micaceous materials: Muscovite-2M1, a comparison with single-crystal structure refinement. *The Canadian Mineralogist*, **34**, 115–122.
MacEwan, D.M.C. and Wilson, J. (1984) Interlayer and intercalation complexes of clay minerals, Chapter 3, pp. 197–248, in: *Crystal Structures of Clay Minerals and Minerals and Their X-Ray Identification* (G.W. Brindley and G. Brown, editors). Mineralogical Society, London.
Maggi, F. (2003) *Influenza Della Composizione del Liquido Interstiziale Sulla Resistenza dei Terreni Argillosi a Struttura Complessa*. Ph.D. thesis in Dottorato di Ricerca in Ingegneria Geotecnica, University of Naples Federico II.
Maggi, F. and Pellegrino, A. (2002) Sperimentazione in sito sul miglioramento della resistenza di un'argilla attiva con modifica del liquido interstiziale. *Incontro Annuale dei Ricercatori di Geotecnica IARG*, 1–4.
Mansour M.F., Morgenstern, N.R., and Martin, C.D. (2011) Expected damage from displacement of slow moving slides. *Landslide*, **8**, 117–131.
Meunier, A., Inoue, A., and Beaufort, D. (1991) Chemiographic analysis of trioctahedral smectite-to-chlorite conversion series from the Ohyu caldera, Japan. *Clays and Clay Minerals*, **39**, 409–415.
Moore, D.M. and Reynolds, R.C., Jr. (1997) X-*ray Diffraction and the Identification and Analysis of Clay Minerals*. Second edition. Oxford University Press, Oxford and New York, 378 pp.
Omosoto, O., McCarty, D.K., Hillier, S., and Kleeberg, R. (2006) Some successful approaches to quantitative mineral analysis as revealed by the 3rd Reynolds Cup contest. *Clays and Clay Minerals*, **54**, 748–760.
Pearson, M.J. (1978) Quantitative clay mineralogical analyses from the bulk chemistry of sedimentary rocks. *Clays and Clay Minerals*, **26**, 423–433.
Phillips, M.W. and Ribbe, P.H. (1973) The structure of monoclinic potassium-rich feldspars, *American Mineralogist*, **58**, 263–270.
P.A.I., Piano per l'assetto idrogeologico (2011) Carta inventario dei fenomeni franosi e della relativa intensità in funzione delle massime velocità attese (scala 1:5000). Autorità di bacino regionale destra sele. Regione Campania.
Picarelli, L. and Russo, C. (2004) Remarks on the mechanisms of slow active landslides and the interaction with man-made works. in: *Proceedings of the IX International Symposium on Landslide Rio de Janeiro, Brazil*, (W. Lacerda, editor) **2**, 1141–1176. DOI: 10.201/b16816–169.

Rule, A.C. and Bailey, S.W. (1987) Refinement of the crystal structure of a monoclinic ferroan clinochlore. *Clays and Clay Minerals*, **35**, 129–138.

Shen, S., Zaidi, S.R., Mutuairi, B.A., Shehry, A.A., Sitepu, H., Hamoud, S.A., Khaldi, F.S., and Edhaim, F.A. (2012) Quantitative XRD bulk and clay mineralogical determination of paleosol section of Unayzah and basal KHUFF clastics in Saudi Arabia. *Powder Diffraction*, **27**, 126–130.

Slaughter, M. (1989) Quantitative determination of clays and other minerals in rocks. Pp. 120–121 in: *Quantitative Mineral Analysis of Clays* (D.R. Pevear and F.A. Mumpton, editors). CMS Workshop Lectures 1. The Clay Minerals Society, Boulder, Colorado, USA.

Smith, D.K., Johnson, G.G., Jr., Scheible, W., Wims, A.M., Johnson J.L., and Ullmann, G. (1987) Quantitative X-ray powder diffraction method using the full diffraction pattern. *Powder Diffraction*, **2**, 73–77.

Snyder, R.L. and Bish, D.L. (1989) Quantitative analysis. Chapter 5, pp. 101–144 in: *Reviews In Mineralogy, Volume 20: Modern Powder Diffraction* (D.L. Bish and J.E. Post, editors.), Mineralogical Society of America, Blacksburg, Virginia, USA.

Son, B.K., Yoshimura, T., and Fukusawa, H. (2001) Diagenesis of dioctahedral and trioctahedral smectite from alternating beds in Miocene to Pleistocene rocks of the Niigata Basin, Japan. *Clays and Clay Minerals*, **49**, 333–346.

Środoń, J. (2002) Quantitative mineralogy of sedimentary rocks with emphasis on clays and with applications to K-Ar dating. *Mineralogical Magazine*, **66**, 677–687.

Środoń, J., Drits, V.A., McCarty, D.K., Hsieh, J.C.C., and Eberl, D.D. (2001) Quantitative X-ray diffraction analysis of clay bearing rocks from random preparation. *Clays and Clay Minerals*, **49**, 514–528.

Takeda, H. and Ross, M. (1975) Mica polytypism: Dissimilarities in the crystal structures of coexisting 1M and 2M1 biotite. *American Mineralogist*, **60**, 1030–1040.

Taylor, R.K. and Cripps, J.C. (1987) Weathering effects: Slopes in mudrocks and over consolidated clay. Chapter 13 in: *Slope Stability* (M.G. Anderson and K.S. Richards, editors) 405–445.

Taylor, R.K. and Spears, D.A. (1981) The breakdown of British coal measure rocks. *International Journal of Rock Mechanics and Mining Sciences*, **7**, 481–501.

Uneno, H., Jige, M., Sakamoto, T., Balce, G.R., and Deguchi, I. (2008) Geology and clay mineralogy of the landslides area in Guisaugon, Southern Leyte Island, Philippines. *University Bulletin of Chiba Institute of Science*, **1**, 9 pp.

Ufer, K., Stanjek, H., Roth, G., Dohrmann, R., Kleeberg, R., and Kaufhold, S. (2008) Quantitative phase analysis of bentonites by the Rietveld method. *Clays and Clay Minerals*, **56**, 272–282.

Ufer, K., Kleeberg, R., Bergmann, J., and Dohrmann, R. (2012) Rietveld refinement of disordered illite-smectite mixed layer structures by a recursive algorithm. II: Powder-pattern refinement and quantitative phase analysis. *Clays and Clay Minerals*, **60**, 535–552.

Velde, B. (1995) *Origin and Mineralogy of Clays: Clays and the Environment*. Edition 1, Springer-Verlag, Berlin, Heidelberg, 334 pp.

(*Received 13 March 2018; revised 30 May 2018; Ms. 1170; AE: R. Dohrmann*)